spectroscopy journal

MDPI

Article

Benchtop ^{19}F Nuclear Magnetic Resonance (NMR) Spectroscopy-Optimized Knorr Pyrazole Synthesis of Celecoxib and Mavacoxib, 3-(Trifluoromethyl) Pyrazolyl Benzenesulfonamides, Non-Steroidal Anti-Inflammatory Drugs (NSAIDs)

Andrew Chyu, Selina Xi, Joshua Kim, Galen Liu, Indalina Chan, Seoyeon Hong, Allen Ke, Thomas Lavery, Anushree Marimuthu, Arjun Akula and Edward Njoo *

Department of Chemistry, Aspiring Scholars Directed Research Program, Fremont, CA 94539, USA
* Correspondence: edward.njoo@asdrp.org

Abstract: Fluorinated organic compounds have demonstrated remarkable utility in medicinal chemistry due to their enhanced metabolic stability and potent therapeutic efficacy. Several examples exist of fluorinated non-steroidal anti-inflammatory drugs (NSAIDs), including diflunisal, flurbiprofen, and trifluoromethylated pyrazoles celecoxib and mavacoxib. These trifluoromethylated pyrazoles, which are most commonly constructed through the cyclocondensation of a trifluorinated 1,3-dicarbonyl and an aryl hydrazine, are also found in numerous other drug candidates. Here, we interrogate the effects of solvents and the presence of Brønsted or Lewis acid catalysts on catalyzing this process. We highlight the utility of benchtop ^{19}F NMR spectroscopy in enabling the real-time quantification of reaction progress and the identification of fluorinated species present in crude reaction mixtures without the need for cost-prohibitive deuterated solvents. Ultimately, we find that the reaction solvent has the greatest impact on the rate and product yield, and also found that the relationship between the keto-enol equilibrium of the dicarbonyl starting material pyrazole formation rate is highly solvent-dependent. More broadly, we describe the optimization of the yield and kinetics of trifluoromethylpyrazole formation in the synthesis of celecoxib and mavacoxib, which is made possible through high-throughput reaction screening on benchtop NMR.

Keywords: benchtop ^{19}F NMR spectroscopy; keto-enol tautomerism; NSAIDs; trifluoromethylated pyrazole; Knorr pyrazole cyclocondensation; organofluorine

Citation: Chyu, A.; Xi, S.; Kim, J.; Liu, G.; Chan, I.; Hong, S.; Ke, A.; Lavery, T.; Marimuthu, A.; Akula, A.; et al. Benchtop ^{19}F Nuclear Magnetic Resonance (NMR) Spectroscopy-Optimized Knorr Pyrazole Synthesis of Celecoxib and Mavacoxib, 3-(Trifluoromethyl) Pyrazolyl Benzenesulfonamides, Non-Steroidal Anti-Inflammatory Drugs (NSAIDs). *Spectrosc. J.* **2024**, *2*, 206–215. https://doi.org/10.3390/spectroscj2040014

Academic Editor: Clemens Burda

Received: 1 October 2024
Revised: 27 October 2024
Accepted: 6 November 2024
Published: 11 November 2024

1. Introduction

Since the initial success of fluorinated corticosteroids in the 1950s and fluoroquinolones in the 1980s, the number of FDA-approved fluorinated pharmaceuticals has steadily increased and now accounts for twenty percent of all FDA-approved pharmaceutical agents [1–6]. This can be attributed to the improved metabolic stability, bioavailability, and therapeutic profiles associated with fluorinated motifs [4–11]. Among these, trifluoromethylated pyrazoles have demonstrated particular pharmacological potency [12–16], being referenced over twenty-six thousand times in patents and peer-reviewed publications concerning the preparation and use of various therapeutics and agrochemicals as of 2024. FDA-approved celecoxib (Celebrex) and EU-approved mavacoxib (Trocoxil), examples of trifluoromethylated pyrazole-containing compounds, are non-steroidal anti-inflammatory drugs (NSAIDs) that act through the inhibition of cyclooxygenase (COX) enzymes that mediate the conversion of arachidonic acid into inflammatory prostaglandins [17–22] (Figure 1A).

Numerous methods have been described for the preparation of these and other fluorinated pyrazoles, including the fluorination of methylpyrazoles using electrophilic or radical fluorination reagents and the fluorination of aminopyrazoles using a Balz–Schiemann

nucleophilic substitution involving a diazonium salt [13,23–26]. However, the most direct and common synthesis involves the Knorr cyclocondensation of 1,3-dicarbonyls and hydrazines [27–30] (Figure 1A). This Knorr synthesis has been industrially applied to the kilogram scale of celecoxib, prepared from the condensation of 4,4,4-trifluoro-1-(4-methylphenyl)butane-1,3-dione and 4-sulfonamidophenylhydrazine [31–33].

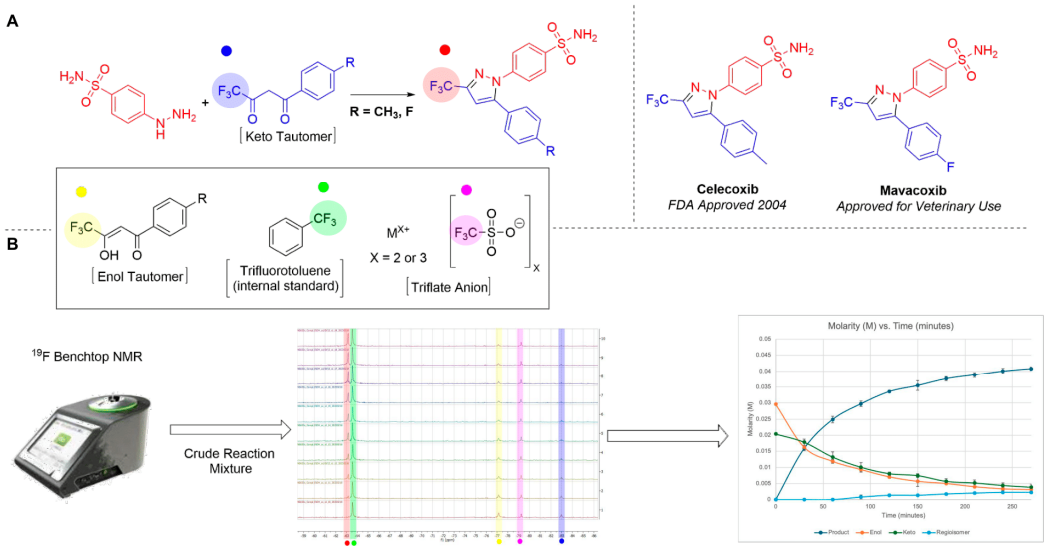

Figure 1. (**A**) Celecoxib and mavacoxib: COX-2-selective NSAIDs containing the pyrazole moiety, prepared through the Knorr pyrazole cyclocondensation of a phenylhydrazine and a 1,3-dicarbonyl compound. (**B**) Workflow for ^{19}F NMR-based mechanistic studies on the Knorr pyrazole cyclocondensation; crude reaction mixtures directly analyzed via ^{19}F NMR (benchtop NMR stock photo adapted with permission. Copyright 2022, Nanalysis Corp).

Lewis and Brønsted acid catalysts have demonstrated broad utility in accelerating various cyclocondensation constructions of heterocycles including Knorr pyrazole synthesis, likely through electrophilic activation by protonation or coordination to the 1,3-dicarbonyl [34–42]. Additionally, Brønsted acids may disrupt the intramolecular hydrogen bonding that stabilizes the less reactive enol tautomer and facilitates the protonation of the electrophilic carbonyl, enhancing its susceptibility to nucleophilic attack by the hydrazine [37–41].

Initial reaction condition screening performed by Reddy et al. has previously demonstrated that the efficiency and yield of the uncatalyzed Knorr pyrazole synthesis in the industrial-scale preparation of celecoxib can be significantly influenced by solvent effects [31]. Our laboratory has previously reported the utility of benchtop ^{19}F NMR spectroscopy in high-throughput condition screening for the reaction optimization and quantitative reaction monitoring of fluorinated pharmaceutical agents [43–45], solvent effects on K_{eq} (keto/enol) of fluorinated dicarbonyls [44], and the mechanistic deconvolution of heterocycle-forming multicomponent cyclocondensation reactions, such as the Biginelli condensation reaction through the real-time quantification of even transient intermediates and products of complex multicomponent reactions that can be directly measured from crude reaction aliquots in non-deuterated solvents [45] (Figure 1B).

Here, we sought to determine the role of solvents and catalysts on the rate and efficiency of trifluoromethylated pyrazole formation and to understand how perturbations of the keto-enol tautomerization equilibrium of the trifluoromethylated 1,3-dicarbonyl starting materials influence the efficiency of pyrazole formation. In this study, we utilize benchtop ^{19}F NMR spectroscopy as a high-throughput condition screening platform to identify the optimal catalyst, solvent, and mechanistic trends in the preparation of two trifluoromethylated pyrazoles: celecoxib and mavacoxib. The presence of the trifluoromethyl motifs conveniently serves as spectroscopic handles with which to quantitatively monitor

reaction kinetics [46–50]. With this workflow, we screened for potential applications of nine common Lewis and Brønsted acid catalysts across a representative selection of protic and aprotic solvents in the preparation of fluorinated pyrazoles from 1,3-dicarbonyl substrates. Through this reaction screening, we identified that pyrazole formation occurs the fastest in dimethylformamide (DMF), irrespective of the presence of Lewis or Brønsted acid catalysts, suggesting that solvents play the most critical role in reaction efficiency. Additionally, we show that the direct effect of keto-enol equilibrium on the reaction rate is most pronounced in polar protic solvents. More broadly, we show the applicability of benchtop ^{19}F NMR spectroscopy as an analytical screening platform that provides rapid, quantitative mechanistic insight into tautomerization and cyclocondensation kinetics without the necessity of deuterated solvents, and which cannot be easily or as rapidly observed through other means. This enables the condition optimization of these and potentially other fluorinated heterocycles.

2. Materials and Methods

2.1. General Synthesis Procedure (Micro-Scale)

To a standard 5 mm NMR tube an initial solution of trifluoromethylated 1,3-dicarbonyl (0.20 mmol/mL), catalyst (0.02 mmol/mL), and solvent (0.25 mL) was added. The reaction mixture was placed into a 60 °C water bath and was allowed to equilibrate over a 30 min period. Another separate solution of 4-sulfonamidophenylhydrazine HCl and solvent (0.20 mmol/mL, 0.25 mL), as well as the addition of α,α,α-trifluorotoluene (0.10 mmol/mL) directly into the reaction mixture as a chemical shift reference and integration standard due to its compatibility with reaction conditions [45], was then added. An initial 60 MHz ^{19}F NMR was taken and the reaction mixture was placed into a 60 °C water bath, and ^{19}F NMR spectra were taken at 30 min intervals over a 4.5 h period with a Nanalysis NMReady 60-Pro benchtop nuclear magnetic resonance spectrometer.

2.2. Kinetic Parameters

Kinetics were run in a water bath heated to a temperature of 60 °C and maintained on a thermocouple heat plate. Data points are reported as the K_{eq} of a single data experiment at which the concentrations of each tautomer reach equilibrium. NMR spectra were taken with a 200 ppm spectral width and a 1.0 s scan delay with 32 scans.

3. Results and Discussion

3.1. Initial Rate

The initial keto-enol equilibration of the fluorinated 1,3-dicarbonyls **2** and **3** under different reaction conditions was found to be dependent on both the solvent and catalyst. Consistent with expectation and with previous reports, solvents capable of hydrogen bonding gave predominantly the ketone tautomer (^{19}F δ = −80 to −84 ppm, depending on the solvent, and assigned by the corresponding ^{1}H NMR (Figure S28)), whereas the enol tautomer (^{19}F δ = −71 to −77 ppm, as assigned by the corresponding ^{1}H NMR (Figure S28)) was observed to dominate the equilibrium in aprotic polar solvents (DMSO, NMP, and DMF). When dicarbonyl **2** or **3** is subjected to reaction with 4-sulfonamidophenylhydrazine **1**, direct conversion into the trifluorinated pyrazole celecoxib **6** or mavacoxib **7** was observed by aliquot reaction ^{19}F NMR (Figure 2); the identity of the product peak by NMR was deemed to be identical to an authentic sample of celecoxib or mavacoxib and verified by liquid chromatography–mass spectrometry (LC-MS) (Figure S27). From these initial solvent investigations, we observed that the formation of both celecoxib and mavacoxib is most rapid in DMF compared to other solvents, while the slowest rates of conversion are observed in ethanol (Figure 2B). Remarkably, there is no generalizable correlation between the solvent-driven solution phase equilibrium constant of the dicarbonyl and the initial rate of pyrazole formation (Figure 3A), though specifically among the two protic solvents screened (methanol and ethanol) a greater K_{eq} in methanol versus ethanol (0.67 vs. 0.24) resulted in a much faster rate of conversion (8.83 μM/s in MeOH, as opposed to 3.33 μM/s

in EtOH). Subsequently, we screened a number of common Brønsted acids, including hydrochloric acid, p-toluenesulfonic acid, and acetic acid, along with five transition metal Lewis acid catalysts, including $LaCl_3$, $Yb(OTf)_3$, $Sc(OTf)_3$, $In(OTf)_3$, $Er(OTf)_3$, and $Cu(OTf)_2$. Within trials performed in protic solvents, this general positive correlation is retained between the K_{eq} and the initial reaction rate (Figure 3B). However, in aprotic solvents, no consistent positive trend is observed consistently across all five solvents (Figure 3C).

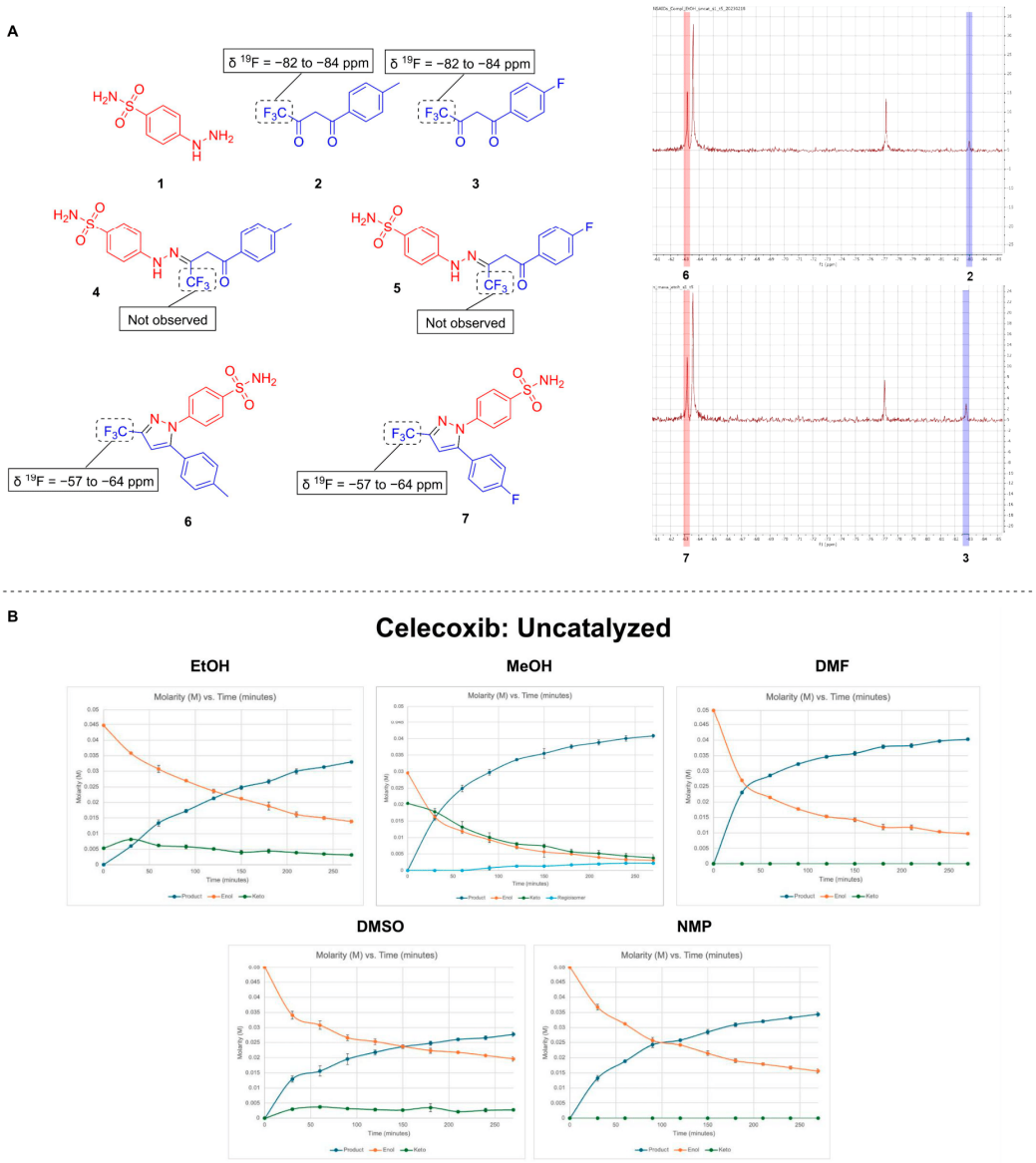

Figure 2. (**A**) Key reaction components in the preparation of celecoxib and mavacoxib and their representative ^{19}F NMR chemical shifts. (**B**) Concentration of product formation and starting dicarbonyl consumption as a function of time in different solvents (Figures S5–S24, Table S1).

It is possible that this behavior of the fluorinated dicarbonyls **2** and **3** in protic solvents (MeOH, EtOH) is attributed to the increased availability of the reactive keto tautomer, which is aligned with the proposed reaction mechanism, which proceeds through an initial nucleophilic attack of the keto tautomer while the enol tautomer remains unreactive at the desired trifluoromethyl ketone center. However, polar aprotic solvents, such as DMF and DMSO, do not strictly follow this trend, demonstrating that the rate of reaction is not solely dependent on the K_{eq}. We attribute this inconsistency in the initial reaction rate to a solvent's ability to stabilize the reaction intermediates by acting as a hydrogen

bond acceptor, such as in DMF. Some notable conditions include $Er(OTf)_3$ and being uncatalyzed in DMF, which have the fastest initial formation of product in celecoxib and mavacoxib, respectively. Additionally, the lack of a keto tautomer present in all polar aprotic solvents, such that K_{eq} is almost zero, highlights the lack of catalyst effects on keto-enol tautomerization and the determinant factor being the solvent.

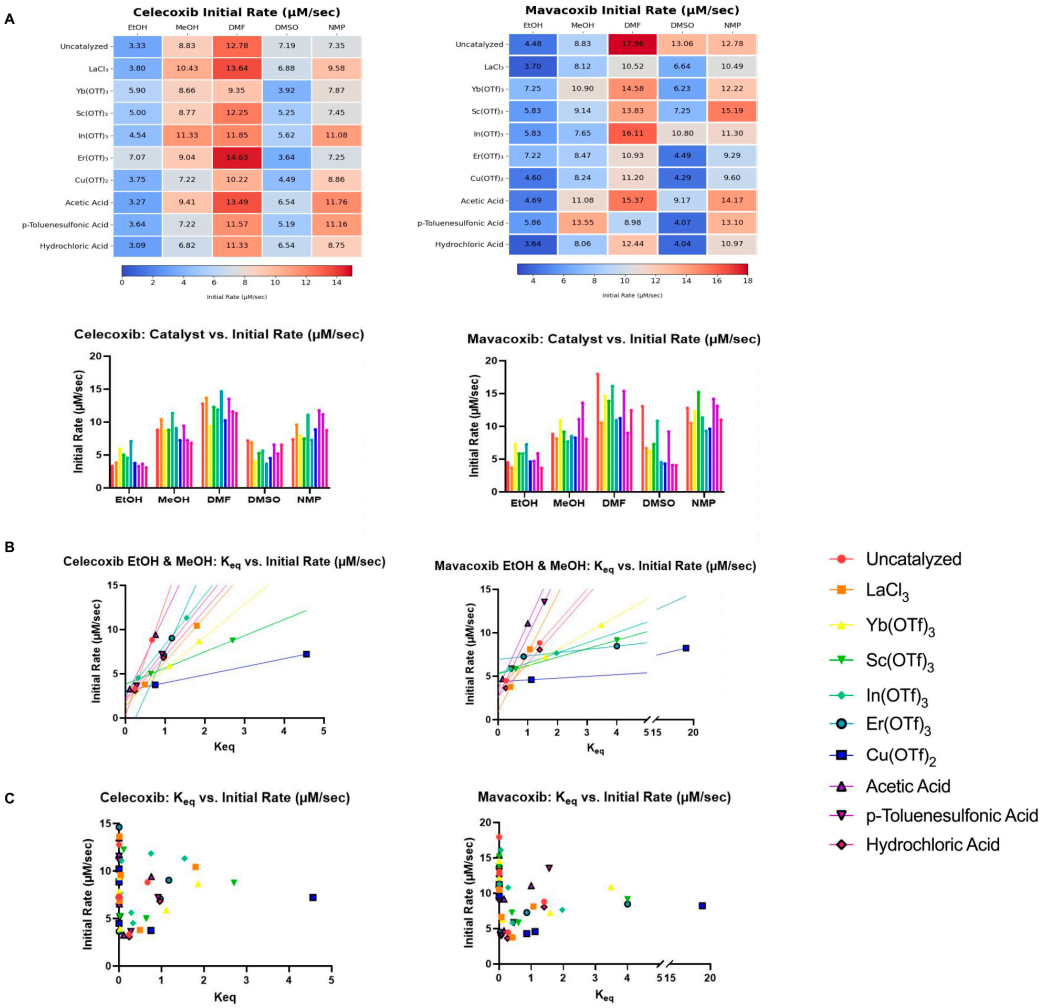

Figure 3. Catalyst and solvent optimization screening of the celecoxib and mavacoxib initial rate (μM/sec). (**A**) Heatmap and bar graph of initial rate (μM/sec) of all solvent and catalyst conditions. (**B**) K_{eq} against initial rate (μM/sec) by catalyst in ethanol and methanol. (**C**) K_{eq} against initial rate (μM/sec) by catalyst in all solvents.

The lack of these observable intermediates by ^{19}F NMR suggests that the initial nucleophilic attack of hydrazine **1** to the trifluoromethylated ketone of **2** or **3** is rate-determining, and that subsequent cyclization through intramolecular condensation from hydrazone **4** or **5** is a much faster process. This is consistent with first-order kinetics observed for both hydrazine and 1,3-dicarbonyl.

3.2. Final Conversion

Irrespective of the presence of a catalyst, methanol conditions resulted in the greatest yield of both compounds (celecoxib: 96%, mavacoxib: >99%), notably $Cu(OTf)_2$ and being uncatalyzed for the formation of celecoxib and mavacoxib, respectively. Consistent with expectation, solvents that favor the keto tautomer result in greater formation of the desired product, which can be attributed to the more efficient formation of the product (Figure 4B). However, despite DMSO and ethanol being able to stabilize the keto tautomer at a higher

rate than NMP and DMF, these conditions have shown the least conversion into celecoxib and mavacoxib, respectively (Figure 4A). The accelerated conversion of intermediate 5 into mavacoxib can be ascribed to its heightened reactivity with the phenylhydrazine starting material. This is likely due to the electron-withdrawing effects of the para-fluorine substituent, which increases the electrophilicity of the 1,3-dicarbonyl, thus promoting nucleophilic attack by the hydrazine.

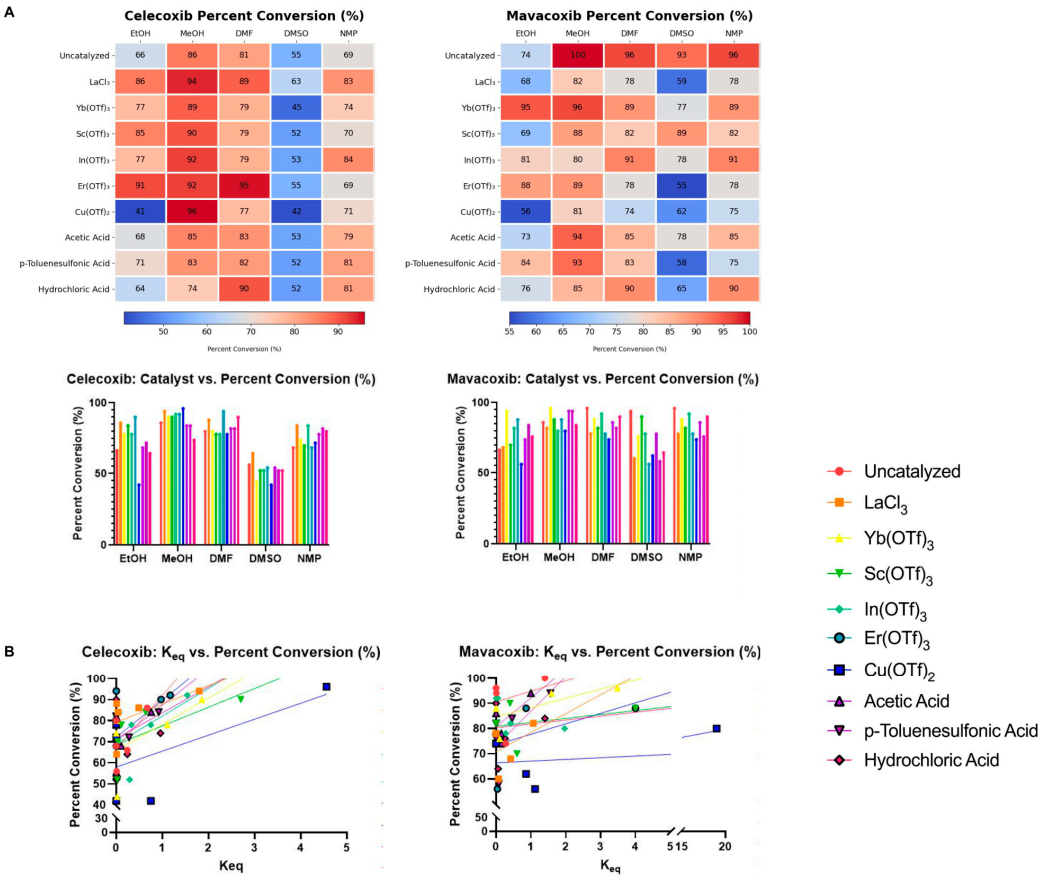

Figure 4. Catalyst and solvent optimization screening of the celecoxib and mavacoxib percent conversion after 4.5 h. (**A**) Heatmap and bar graph of percent conversion (%) of all solvent and catalyst conditions. (**B**) K_{eq} against percent conversion (%) by catalyst in all solvents.

3.3. Regioisomer

Previously, the undesired 1,3-aryl regioisomers of **1G** have been reported as a byproduct (^{19}F $\delta = -58.85$ ppm in methanol) [31], most likely resulting from a nucleophilic attack of the hydrazine to the less electrophilic aryl ketone rather than the trifluoromethyl ketone (Figure 5). We observed the formation of this regioisomer exclusively when the reaction was conducted in methanol. The formation of the regioisomer is attributed to the competing nucleophilicity of solvents such as methanol and ethanol; however, this phenomenon is not observed in ethyl or isopropyl alcohol solvents, presumably due to their greater steric bulk, resulting in decreased favorability of the formation of these solvates. Therefore, we attribute the formation of the regioisomer to methanol being added to the 3-dicarbonyl, forming a dimethyl acetal, and thereby reducing electrophilicity at that site, forcing a nucleophilic attack by the hydrazine on the 1-dicarbonyl **1A** (Figure 5). Additionally, the formation of the regioisomer is not catalytically affected and not consistent across both compounds (Table 1).

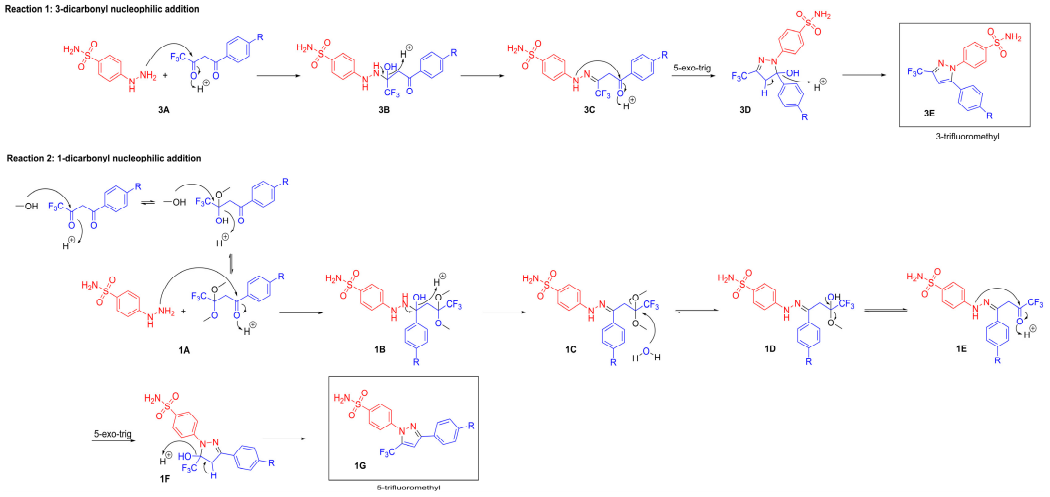

Figure 5. Mechanism for the formation of fluorinated pyrazoles and their regioisomers. (1) The phenylhydrazine condenses with the 3-dicarbonyl to form the hydrazone intermediate **3C**. This undergoes a 5-exo-trig cyclization **3D** with subsequent dehydration to form the 3-trifluoromethyl pyrazole **3E**. (2) The 1,3-dicarbonyl is in equilibrium with the dimethoxy intermediate **1A**. The phenylhydrazine condenses with the 3-hydroxy-3-methoxy intermediate carbonyl to form the hydrazone dimethyl acetal intermediate **1C**. This is in equilibrium with the hydrazone intermediate **1E**, which undergoes a 5-exo-trig cyclization with subsequent dehydration to form the 5-trifluoromethyl regioisomer **1G**.

Table 1. Percent of the regioisomer observed after 4.5 h.

Catalyst	Celecoxib	Mavacoxib
Uncatalyzed	4.5%	0.0%
$LaCl_3$	3.2%	2.8%
$Yb(OTf)_3$	2.2%	3.0%
$Sc(OTf)_3$	3.9%	4.0%
$In(OTf)_3$	4.4%	3.2%
$Er(OTf)_3$	3.4%	3.3%
$Cu(OTf)_2$	2.5%	2.7%
Acetic acid	4.4%	3.3%
p-toluenesulfonic acid	3.9%	3.7%
Hydrochloric acid	2.7%	3.6%

4. Conclusions

In summary, we demonstrate through benchtop ^{19}F NMR that the kinetics of the Knorr pyrazole cyclocondensation of trifluorinated diketones and aryl hydrazines towards the preparation of celecoxib and mavacoxib are heavily influenced by reaction solvents over the presence of Lewis or Brønsted acid catalysts. In the protic solvents screened in this study, the rate of pyrazole formation was found to be directly dependent on the relative concentration of the 1,3-dicarbonyl ketone tautomer in solution. We observed that the aprotic solvents DMF and NMP favor the initial formation of celecoxib and mavacoxib, while the protic solvent methanol results in greater overall conversion. Additionally, we found minimal to no consistent catalytic effect of both Lewis and Brønsted acids on the initial rate and total product formation. This trend might be attributed to the differences in each solvent to stabilize key reaction intermediates.

Ultimately, we demonstrated the utility of benchtop ^{19}F NMR for real-time kinetic analysis for high-throughput condition screening in the preparation of two trifluoromethylated phenylpyrazoles of pharmaceutical importance. Beyond the preparation of celecoxib and mavacoxib, the workflow for high-throughput solvent and catalyst screening described

here is broadly applicable to the synthesis of other heterocyclic constructions containing key fluorinated motifs.

Supplementary Materials: The following supporting information can be downloaded at: https://www.mdpi.com/article/10.3390/spectroscj2040014/s1, Figure S1. K_{eq} vs. initial rate (μM/sec), five solvents, celecoxib; Figure S2. K_{eq} vs. initial rate (μM/sec), five solvents, mavacoxib; Figure S3. K_{eq} vs. product (M), five solvents, celecoxib; Figure S4. K_{eq} vs. product (M), five solvents, mavacoxib; Figure S5. Molarity of components after 4.5 h, celecoxib uncatalyzed; Figure S6. Molarity of components after 4.5 h, celecoxib $LaCl_3$; Figure S7. Molarity of components after 4.5 h, celecoxib $Yb(OTf)_3$; Figure S8. Molarity of components after 4.5 h, celecoxib $Sc(OTf)_3$; Figure S9. Molarity of components after 4.5 h, celecoxib $In(OTf)_3$; Figure S10. Molarity of components after 4.5 h, celecoxib $Er(OTf)_3$; Figure S11. Molarity of components after 4.5 h, celecoxib $Cu(OTf)_2$; Figure S12. Molarity of components after 4.5 h, celecoxib acetic acid; Figure S13. Molarity of components after 4.5 h, celecoxib p-toluenesulfonic acid; Figure S14. Molarity of components after 4.5 h, celecoxib hydrochloric acid; Figure S15. Molarity of components after 4.5 h, mavacoxib uncatalyzed; Figure S16. Molarity of components after 4.5 h, mavacoxib $LaCl_3$; Figure S17: Molarity of components after 4.5 h, mavacoxib $Yb(OTf)_3$; Figure S18. Molarity of components after 4.5 h, mavacoxib $Sc(OTf)_3$; Figure S19. Molarity of components after 4.5 h, mavacoxib $In(OTf)_3$; Figure S20. Molarity of components after 4.5 h, mavacoxib $Er(OTf)_3$; Figure S21: Molarity of components after 4.5 h, mavacoxib $Cu(OTf)_2$; Figure S22. Molarity of components after 4.5 h, mavacoxib acetic acid; Figure S23. Molarity of components after 4.5 h, mavacoxib p-toluenesulfonic acid; Figure S24. Molarity of components after 4.5 h, mavacoxib hydrochloric acid; Figure S25. Negative ln of molarity from 0.5 h to 4.5 h in methanol, uncatalyzed; Figure S26. Authentic standard of celecoxib compared to a crude reaction mixture of celecoxib in MeOH, uncatalyzed after 4.5 h on benchtop ^{19}F NMR; Figure S27. Authentic standard of celecoxib compared to a crude reaction mixture of celecoxib in MeOH, uncatalyzed on LC-MS; Figure S28. 4,4,4-trifluoro-1-(4-methylphenyl)butane-1,3-dione over 1.5 h with initial and final ^{19}F NMR in CD_3OD and $CDCl_3$; Table S1. ^{19}F chemical shifts.

Author Contributions: Conceptualization, A.K., A.M., A.A. and E.N.; methodology, A.K., A.M. and E.N.; investigation, A.C., S.X., J.K., G.L., I.C., S.H., A.K., T.L., A.M. and A.A.; writing—original draft preparation, A.C., S.X., J.K., G.L. and E.N.; writing—review and editing, A.C., S.X., J.K., G.L. and E.N. All authors have read and agreed to the published version of the manuscript.

Funding: This research was funded by the Olive Children Foundation.

Institutional Review Board Statement: Not applicable.

Informed Consent Statement: Not applicable.

Data Availability Statement: The raw data supporting the conclusions of this article will be made available by the authors upon request.

Acknowledgments: The authors thank ASDRP for supporting this research. The authors further gratefully acknowledge Nanalysis Corp. for their support in the incorporation of benchtop NMR in this study.

Conflicts of Interest: The authors declare no conflicts of interest.

References

1. Sheikhi, N.; Bahraminejad, M.; Saeedi, M.; Mirfazli, S.S. A review: FDA-approved fluorine-containing small molecules from 2015 to 2022. *Eur. J. Med. Chem.* **2023**, *260*, 115758. [CrossRef] [PubMed]
2. Inoue, M.; Sumii, Y.; Shibata, N. Contribution of Organofluorine Compounds to Pharmaceuticals. *ACS Omega* **2020**, *5*, 10633–10640. [CrossRef] [PubMed]
3. Zhou, Y.; Wang, J.; Gu, Z.; Wang, S.; Zhu, W.; Aceña, J.L.; Soloshonok, V.A.; Izawa, K.; Liu, H. Next Generation of Fluorine-Containing Pharmaceuticals, Compounds Currently in Phase II–III Clinical Trials of Major Pharmaceutical Companies: New Structural Trends and Therapeutic Areas. *Chem. Rev.* **2016**, *116*, 422–518. [CrossRef] [PubMed]
4. Shabir, G.; Saeed, A.; Zahid, W.; Naseer, F.; Riaz, Z.; Khalil, N.A.; Muneeba; Alberício, F. Chemistry and Pharmacology of Fluorinated Drugs Approved by the FDA (2016–2022). *Pharmaceuticals* **2023**, *16*, 1162. [CrossRef]
5. Johnson, B.M.; Shu, Y.-Z.; Zhuo, X.; Meanwell, N.A. Metabolic and Pharmaceutical Aspects of Fluorinated Compounds. *J. Med. Chem.* **2020**, *63*, 6315–6386. [CrossRef]

6. O'Hagan, D.; Young, R.J. Future Challenges and Opportunities with Fluorine in Drugs? *Med. Chem. Res.* **2023**, *32*, 1231–1234. [CrossRef]
7. Niu, Z.-X.; Hu, J.; Sun, J.-F.; Wang, Y.-T. Fluorine in the Pharmaceutical Industry: Synthetic Approaches and Application of Clinically Approved Fluorine-Enriched Anti-Infectious Medications. *Eur. J. Med. Chem.* **2024**, *271*, 116446. [CrossRef]
8. Henary, E.; Casa, S.; Dost, T.L.; Sloop, J.C.; Henary, M. The Role of Small Molecules Containing Fluorine Atoms in Medicine and Imaging Applications. *Pharmaceuticals* **2024**, *17*, 281. [CrossRef]
9. Barnes-Seeman, D.; Beck, J.; Springer, C. Fluorinated Compounds in Medicinal Chemistry: Recent Applications, Synthetic Advances and Matched-Pair Analyses. *Curr. Top. Med. Chem.* **2014**, *14*, 855–864. [CrossRef]
10. Hagmann, W.K. The Many Roles for Fluorine in Medicinal Chemistry. *J. Med. Chem.* **2008**, *51*, 4359–4369. [CrossRef]
11. Gillis, E.P.; Eastman, K.J.; Hill, M.D.; Donnelly, D.J.; Meanwell, N.A. Applications of Fluorine in Medicinal Chemistry. *J. Med. Chem.* **2015**, *58*, 8315–8359. [CrossRef] [PubMed]
12. Karrouchi, K.; Radi, S.; Ramli, Y.; Taoufik, J.; Mabkhot, Y.; Al-aizari, F.; Ansar, M. Synthesis and Pharmacological Activities of Pyrazole Derivatives: A Review. *Molecules* **2018**, *23*, 134. [CrossRef] [PubMed]
13. Mykhailiuk, P.K. Fluorinated Pyrazoles: From Synthesis to Applications. *Chem. Rev.* **2020**, *121*, 1670–1715. [CrossRef] [PubMed]
14. Khan, M.F.; Alam, M.M.; Verma, G.; Akhtar, W.; Akhter, M.; Shaquiquzzaman, M. The Therapeutic Voyage of Pyrazole and Its Analogs: A Review. *Eur. J. Med. Chem.* **2016**, *120*, 170–201. [CrossRef] [PubMed]
15. Ansari, A.; Ali, A.; Asif, M.; Shamsuzzaman. Review: Biologically Active Pyrazole Derivatives. *New J. Chem.* **2016**, *41*, 16–41. [CrossRef]
16. Du, Y.; Li, G.; Cheng, Y.; Han, C.; Song, C.; Huang, N. Pyrazole-Containing Pharmaceuticals: Target, Pharmacological Activity, and Their SAR Studies. *RSC Med. Chem.* **2022**, *13*, 1300–1321. [CrossRef]
17. Ghlichloo, I.; Gerriets, V. *Nonsteroidal Anti-Inflammatory Drugs (NSAIDs)*; StatPearls: Treasure Island, FL, USA, 2023. Available online: https://www.ncbi.nlm.nih.gov/books/NBK547742/ (accessed on 30 September 2024).
18. Dhondt, L.; Devreese, M.; Croubels, S.; De Baere, S.; Haesendonck, R.; Goessens, T.; Gehring, R.; De Backer, P.; Antonissen, G. Comparative Population Pharmacokinetics and Absolute Oral Bioavailability of COX-2 Selective Inhibitors Celecoxib, Mavacoxib and Meloxicam in Cockatiels (*Nymphicus Hollandicus*). *Sci. Rep.* **2017**, *7*, 12043. [CrossRef]
19. Gong, L.; Thorn, C.F.; Bertagnolli, M.M.; Grosser, T.; Altman, R.B.; Klein, T.E. Celecoxib Pathways. *Pharmacogenetics Genom.* **2012**, *22*, 310–318. [CrossRef]
20. Miller, S.B. Prostaglandins in Health and Disease: An Overview. *Semin. Arthritis Rheum.* **2006**, *36*, 37–49. [CrossRef]
21. Qureshi, O.; Dua, A. *COX Inhibitors*; StatPearls: Treasure Island, FL, USA, 2024. Available online: https://www.ncbi.nlm.nih.gov/books/NBK549795/ (accessed on 30 September 2024).
22. Zarghi, A.; Arfaei, S. Selective COX-2 Inhibitors: A Review of Their Structure-Activity Relationships. *Iran. J. Pharm. Res.* **2011**, *10*, 655–683.
23. Levchenko, V.; Dmytriv, Y.V.; Tymtsunik, A.V.; Liubchak, K.; Rudnichenko, A.; Melnyk, A.V.; Veselovych, S.Y.; Borodulin, Y.V.; Otsalyuk, O.M.; Tolmachev, A.A.; et al. Preparation of 5-Fluoropyrazoles from Pyrazoles and N-Fluorobenzenesulfonimide (NFSI). *J. Org. Chem.* **2018**, *83*, 3265–3274. [CrossRef]
24. Bonacorso, H.; Pittaluga, E.; Porte, L.; Libero, F.; Junges, A.; Zanatta, N.; Martins, M. Unexpected Metal-Free Fluorination and Oxidation at the C-4 Position of Pyrazoles Promoted by Selectfluor. *Synlett* **2015**, *26*, 2009–2013. [CrossRef]
25. Breen, J.; Sandford, G.; Patel, B.; Fray, J. Synthesis of 4,4-Difluoro-^{1}H-pyrazole Derivatives. *Synlett* **2014**, *26*, 51–54. [CrossRef]
26. Fabra, F.; Vilarrasa, J.; Coll, J. Fluoroazoles. III. Synthesis and ^{1}H and ^{19}F NMR Spectra of 3-, 4-, and 5-Fluoro-1-Methylpyrazole. *J. Heterocycl. Chem.* **1978**, *15*, 1447–1449. [CrossRef]
27. Joseph, C.S.; Cory, H.; Maged, H. Selective Incorporation of Fluorine in Pyrazoles. *Eur. J. Org. Chem.* **2015**, *2015*, 3405–3422. [CrossRef]
28. Ohtsuka, Y.; Uraguchi, D.; Yamamoto, K.; Tokuhisa, K.; Yamakawa, T. Syntheses of 2-(Trifluoromethyl)-1,3-Dicarbonyl Compounds through Direct Trifluoromethylation with CF3I and Their Application to Fluorinated Pyrazoles Syntheses. *Tetrahedron* **2012**, *68*, 2636–2649. [CrossRef]
29. Flood, D.T.; Hintzen, J.C.J.; Bird, M.J.; Cistrone, P.A.; Chen, J.S.; Dawson, P.E. Leveraging the Knorr Pyrazole Synthesis for the Facile Generation of Thioester Surrogates for Use in Native Chemical Ligation. *Angew. Chem. Int. Ed.* **2018**, *57*, 11634–11639. [CrossRef]
30. Hassani, A.E.; Rouzi, K.; Assila, H.; Karrouchi, K.; Ansar, M.H. Recent Advances in the Synthesis of Pyrazole Derivatives: A Review. *Reactions* **2023**, *4*, 478–504. [CrossRef]
31. Reddy, A.R.; Sampath, A.; Goverdhan, G.; Yakambaram, B.; Mukkanti, K.; Reddy, P.P. An Improved and Scalable Process for Celecoxib: A Selective Cyclooxygenase-2 Inhibitor. *Org. Process Res. Dev.* **2008**, *13*, 98–101. [CrossRef]
32. Sthalam, V.K.; Singh, A.K.; Pabbaraja, S. An Integrated Continuous Flow Micro-Total Ultrafast Process System (μ-TUFPS) for the Synthesis of Celecoxib and Other Cyclooxygenase Inhibitors. *Org. Process Res. Dev.* **2019**, *23*, 1892–1899. [CrossRef]
33. Scholtz, C.; Riley, D.L. Improved batch and flow syntheses of the nonsteroidal anti-inflammatory COX-2 inhibitor celecoxib. *React. Chem. Eng.* **2021**, *6*, 138–146. [CrossRef]
34. Sloop, J.C.; Bumgardner, C.L.; Washington, G.; Loehle, W.D.; Sankar, S.S.; Lewis, A.B. Keto–Enol and Enol–Enol Tautomerism in Trifluoromethyl-β-Diketones. *J. Fluor. Chem.* **2006**, *127*, 780–786. [CrossRef]

35. Medjahed, N.; Kibou, Z.; Berrichi, A.; Choukchou-Braham, N. Advances in Pyrazoles Rings' Syntheses by Heterogeneous Catalysts, Ionic Liquids, and Multicomponent Reactions-A Review. *Curr. Org. Chem.* **2023**, *27*, 471–509. [CrossRef]
36. Jia, Q.; Li, Y.; Lin, Y.; Ren, Q. The Combination of Lewis Acid with N-Heterocyclic Carbene (NHC) Catalysis. *Catalysts* **2019**, *9*, 863. [CrossRef]
37. Nasseri, M.A.; Salimi, M.; Esmaeili, A.A. Cellulose Sulfuric Acid as a Bio-Supported and Efficient Solid Acid Catalyst for Synthesis of Pyrazoles in Aqueous Medium. *RSC Adv.* **2014**, *4*, 61193–61199. [CrossRef]
38. Ponra, S.; Majumdar, K.C. Brønsted Acid-Promoted Synthesis of Common Heterocycles and Related Bio-Active and Functional Molecules. *RSC Adv.* **2016**, *6*, 37784–37922. [CrossRef]
39. Portilla-Zúñiga, O.; Bautista-Aguilera, Ó.M.; Martínez, J.J.; Rojas, H.; Macías, M.A.; Iriepa, I.; Romanelli, G.P. Synthesis of N-Substituted Pyrroles Catalyzed by Low-Cost and Commercially Available Aluminas. *Catalysts* **2023**, *13*, 603. [CrossRef]
40. Sanz, R.; Miguel, D.; Martínez, A.; Álvarez-Gutiérrez, J.M.; Rodríguez, F. Brønsted Acid-Catalyzed Benzylation of 1,3-Dicarbonyl Derivatives. *Org. Lett.* **2007**, *9*, 2027–2030. [CrossRef]
41. Motokura, K.; Fujita, N.; Mori, K.; Mizugaki, T.; Ebitani, K.; Kaneda, K. Brønsted Acid Mediated Heterogeneous Addition Reaction of 1,3-Dicarbonyl Compounds to Alkenes and Alcohols. *Angew. Chem. Int. Ed.* **2006**, *45*, 2605–2609. [CrossRef]
42. Danbo, X.; Dan, S.; Qiliang, C.; Jiaqi, Z.; Xiaofei, Z.; Guofu, Z. N-Heterocyclic Carbene/Lewis Acid Catalyzed Enantioselective Aerobic Annulation of α,β-Unsaturated Aldehydes with 1,3-Dicarbonyl Compounds. *J. Org. Chem.* **2016**, *81*, 6136–6141. [CrossRef]
43. Wang, X.; Vu, J.; Luk, C.; Njoo, E. Benchtop ^{19}F nuclear magnetic resonance spectroscopy enabled kinetic studies and optimization of the synthesis of carmofur. *Can. J. Chem.* **2023**, *101*, 518–524. [CrossRef]
44. Udgaonkar, A.; Wu, J.; Rao, A.; Njoo, E. Deuterated Solvent Effects in the Kinetics and Thermodynamics of Keto-Enol Tautomerization of ETFAA. *J. Emerg. Investig.* **2022**, *5*. [CrossRef] [PubMed]
45. Chen, R.; Singh, P.; Su, S.; Kocalar, S.; Wang, X.; Mandava, N.; Venkatesan, S.; Ferguson, A.; Rao, A.; Le, E.; et al. Benchtop 19F Nuclear Magnetic Resonance (NMR) Spectroscopy Provides Mechanistic Insight into the Biginelli Condensation toward the Chemical Synthesis of Novel Trifluorinated Dihydro- and Tetrahydropyrimidinones as Antiproliferative Agents. *ACS Omega* **2023**, *8*, 10545–10554. [CrossRef] [PubMed]
46. Cook, A.G.; Feltman, P.M. Correction to Determination of Solvent Effects on Keto−Enol Equilibria of 1,3-Dicarbonyl Compounds Using NMR. *J. Chem. Educ.* **2010**, *87*, 678–679. [CrossRef]
47. Grootveld, M.; Percival, B.; Gibson, M.; Osman, Y.; Edgar, M.; Molinari, M.; Mather, M.L.; Casanova, F.; Wilson, P.B. Progress in Low-Field Benchtop NMR Spectroscopy in Chemical and Biochemical Analysis. *Anal. Chim. Acta* **2019**, *1067*, 11–30. [CrossRef]
48. Yu, H.-Y.; Myoung, S.; Ahn, S. Recent Applications of Benchtop Nuclear Magnetic Resonance Spectroscopy. *Magnetochemistry* **2021**, *7*, 121. [CrossRef]
49. Archambault, C.M.; Leadbeater, N.E. A Benchtop NMR Spectrometer as a Tool for Monitoring Mesoscale Continuous-Flow Organic Synthesis: Equipment Interface and Assessment in Four Organic Transformations. *RSC Adv.* **2016**, *6*, 101171–101177. [CrossRef]
50. Giberson, J.; Scicluna, J.; Legge, N.; Longstaffe, J. Chapter Three—Developments in benchtop NMR spectroscopy 2015–2020. *Annu. Rep. NMR Spectrosc.* **2021**, *102*, 153–246. [CrossRef]